Synthesis by native chemical ligation and characterization of the scorpion toxin AmmTx3

Claude Zoukimian, Hervé Meudal, Stephan de Waard, Karima Ait Ouares, Sébastien Nicolas, Marco Canepari, Rémy Beroud, Céline Landon, Michel de Waard, Didier Boturyn

Synthesis by native chemical ligation and characterization of the scorpion toxin AmmTx3

Claude Zoukimian[a,b], Hervé Meudal[c], Stephan De Waard[d], Karima Ait Ouares[e], Sébastien Nicolas[d], Marco Canepari[e], Rémy Béroud[b], Céline Landon[c,*], Michel De Waard[d,*] and Didier Boturyn[a,*]

[a] *Department of Molecular Chemistry, Univ. Grenoble Alpes, CNRS, 570 rue de la chimie, CS 40700, Grenoble 38000, France*
[b] *Smartox Biotechnology, 6 rue des platanes, Saint Egrève 38120, France*
[c] *Center for Molecular Biophysics, CNRS, rue Charles Sadron, CS 80054, Orléans 45071, France*
[d] *Institut du Thorax, INSERM, CNRS, Univ. Nantes, 8 quai Moncousu, BP 70721, Nantes 44007, France*
[e] *Laboratory for Interdisciplinary Physics, Univ. Grenoble Alpes, CNRS, 140 Avenue de la Physique, BP 87, Saint-Martin d'Hères 38402, France*

ABSTRACT

The scorpion toxin AmmTx3 is a specific blocker of Kv4 channels. It was shown to have interesting potential for neurological disorders. In this study, we report the first chemical synthesis of AmmTx3 by using the native chemical ligation strategy and validate its biological activity. We determined its 3D structure by nuclear magnetic resonance spectroscopy, and pointed out that AmmTx3 possesses the well-known CSαβ structural motif, which is found in a large number of scorpion toxins. Overall, this study establishes an easy synthetic access to biologically active AmmTx3 toxin.

Introduction

An increasing number of toxins are isolated from various animal venoms and become key molecular compounds for biomedical applications such as cardiovascular diseases,[1] treatment of pain,[2] multiple sclerosis [3] and diabetes.[4] These toxins are mainly produced by micro-organisms, such as bacteria and fungi. Interestingly, the discovery of specific blockers has significantly contributed to the understanding of the involvement of distinct ion channels to cellular and tissue function and pathology. In particular, several potassium channels have been identified as promising therapeutic targets.[5]

In this context, the AmmTx3 toxin identified from the venom of the scorpion *Androctonus mauretanicus*, is a specific blocker of K_v4 channels and was found to reduce Parkinsonian-like motor symptoms and, emotional and cognitive

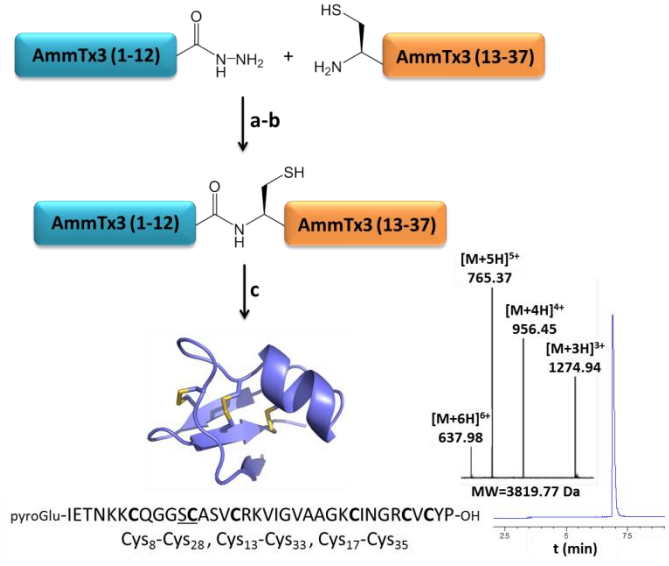

Scheme 1. Synthesis of AmmTx3 using NCL of two peptide segments. a) AmmTx3(1-12) activation: Gn-HCl (6 M), sodium phosphate (0.2 M, pH 3.0), $NaNO_2$ (10 equiv.), -15°C ; b) Ligation : AmmTx3(13-37), MPAA (100 equiv.), pH 6.5, room temperature ; c) Folding and disulfide formation: Tris (0.2 M, pH 8.2). Analytical RP-HPLC (λ = 214 nm) and ES-MS for the final purified AmmTx3 toxin were performed. Observed mass 3819.77 Da *vs* calculated mass 3819.87 Da. MPAA = 4-Mercaptophenylacetic acid; Tris = Tris(hydroxymethyl)aminomethane.

symptoms.[6] Curiously, it was less active on recombinant K_v4 channels and it was explained that auxiliary subunits may contribute to the pharmacological action of the peptide.[7] This toxin protein has a polypeptide chain of 37 amino acid residues with 6 cysteines that forms 3 disulfide bonds. Initially AmmTx3 was isolated from the venom.[8] In order to better characterize this toxin, chemical synthesis was preferred as it avoids venom extraction and purification from natural sources, and provides much larger amounts of toxins. In addition, it paves the way for the production of interesting analogues. As solid phase peptide synthesis (SPPS) presents limitations in the production of peptides of more than 50 amino acids or containing "difficult sequences", convergent synthetic strategies such as the native chemical ligation (NCL) of short fragments are usually used.[9] Additionally, this strategy allows the introduction of segmental isotopic or fluorescent labeling of proteins.[10] To date, recent methods of NCL were developed.[11,12] The use of crypto-thioesters remains a convenient strategy as Fmoc-based SPPS can be exploited to prepare peptide fragments avoiding the handling of strong acids such as hydrogen fluoride used during the Boc strategy.

We herein report the first chemical synthesis of biologically active AmmTx3 by using peptide hydrazide as crypto-thioester.[13] As its structure was not determined to date, we also report the 3D structure of AmmTx3 by using homo- and heteronuclear 2D nuclear magnetic resonance (NMR) spectroscopy.

1. Results and discussion

1.1. Synthesis of AmmTx3

To our knowledge, AmmTx3 was mainly produced by biotechnology. To enable structural studies, chemical synthesis may be used to obtain enough amounts of pure toxin. As predicted, first attempt using standard Fmoc-based SPPS to produce the toxin gave very low yield (See the Supporting Information).[14] We then decided to use the NCL of two short peptide fragments (scheme 1). AmmTx3 contains six cysteine residues that could serve as potential sites for ligation. As the ligation rate between Val and Cys is known to be very low,[12,15] we preferred to carry out the ligation at the Ser–Cys site by using the hydrazide-based NCL.[12]

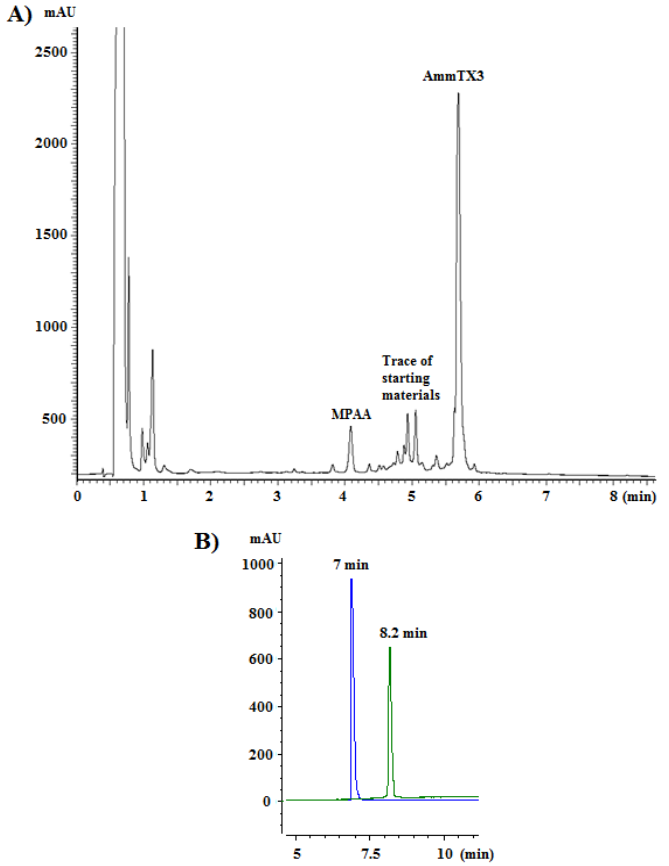

Figure 1. A) HPLC trace at t = 18 h of the NCL reaction; B) Overlapping of unfolded AmmTx3 (green) and folded AmmTx3 (blue) HPLC traces. The absorbance was measured at 214 nm.

In this context, AmmTx3(1-12) peptide was first prepared starting with hydrazine resin using standard Fmoc protocols.[16] The pure fragment was obtained in an excellent 90% overall yield. In parallel, thiol containing-AmmTx3(13-

37) peptide was produced using the SPPS in a moderate 30% overall yield. Prior to the NCL, sodium nitrite was used to produce AmmTx3(1-12) peptide azide at low pH and low temperature.[17] The thiol containing-AmmTx3(13-37) peptide segment was then added and the pH value was adjusted to 6.5 to initiate the native chemical ligation at room temperature. The reaction was monitored by RP-HPLC (Figure 1 A).[18] This methodology is relatively simple to operate, and the overall isolated yield based on resin loading is higher (15% from C-term fragment) than the previous linear SPPS (4%).

Finally, folding and disulphide formation was carried out under alkaline conditions (Tris buffer, pH 8.2). Peptide folding was monitored by RP-HPLC (Figure 1 B) [19] and purification by RP-HPLC gave AmmTx3 toxin that was characterized by ES-MS analysis (Scheme 1, see also the Supporting Information). Experimentally determined molecular weight (MW = 3819.77) was found in excellent agreement with the calculated value (MW = 3819.87).

1.2. Structural determination of AmmTx3

The AmmTx3 in hand, a nuclear magnetic resonance (NMR) study was performed to determine AmmTx3 3D structure. The dispersion of the resonances is good, illustrating that AmmTx3 was well-folded, and all the NH groups are visible on homonuclear spectra except for Asn^5 (see also the Supporting Information). All ^{15}N resonances could be assigned from the ^{1}H-^{15}N heteronuclear multiple-quantum correlation (HMQC) [20] except for Asn^5 and Gly^{10}. ^{1}H and ^{15}N chemical shifts have been deposited in the BioMagResBank (http://www.brmb.wisc.edu) under the entry code 34268. Two sets of NMR spectra were recorded for AmmTx3 prepared from the NCL (AmmTx3-NCL) in comparison with AmmTx3 prepared from classical SPPS (AmmTx3). Chemical shifts of both samples are identical, as highlighted by the superimposition of their HMQC spectra (Figure 2), signifying that the synthetic route does not interfere with the 3D structure of the molecule.

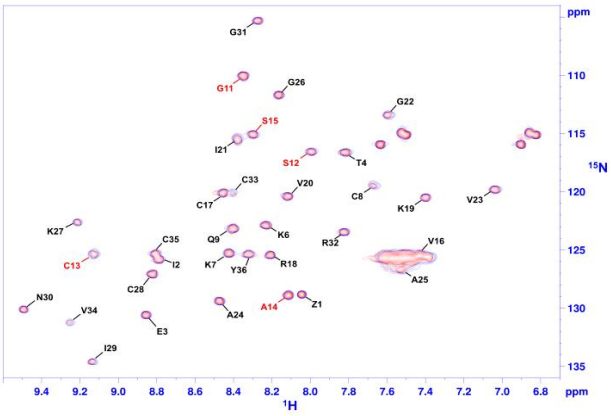

Figure 2. Superimposition of the ^{1}H-^{15}N SoFast-HMQC (natural abundance, 700 MHz with cryoprobe) of AmmTx3-NCL (red) and AmmTx3 (blue). The assignment of each residue is depicted (for clarity side-chain assignments are not indicated). Residues G11 to S15 corresponding to the area of ligation are annotated in red.

The NOE (nuclear overhauser effect) data set used in the final ARIA (ambiguous restraints for iterative assignment) run includes 994 distance restraints (Table 1), with an average of about 28 restraints per residue. Among these restraints, 748 are non-ambiguous. Moreover, during the iterative ARIA procedure, additional constraints were introduced: covalent bonds between sulphur atoms involved in each defined bridge (C8-C28, C13-C33, C17-C35), and 10 H-bond constraints observed within the β-strands.

The 10 selected structures representative of the solution structure of AmmTx3 display small potential energy values, respect all the experimental data and are in agreement with standard covalent geometry (Table 1). The root mean square deviations (RMSD) are low, no experimental distance constraint violation greater than 0.3 Å is observed and the Ramachandran plot exhibits 100% of the (ϕ,ψ) angles in the most favoured regions. The coordinates of this ensemble of structures have been deposited in the Protein Data Bank (http://www.pdb.org) with the entry code 6GGZ.

Table 1. Experimental NMR data used for the calculations, and final structural statistics for the ten models representative of the solution structure of AmmTx3.

NMR constraints	
Distance restraints	
Total NOE	994
Unnambiguous	748
Hydrogen bonds	10
Disulfide bridges[a]	C8-C28, C13-C33, C17-C35
Structural statistics (PDB code 6GGZ)	
Average violations per structure	
NOEs ≥ 0.3 Å	0
Hydrogen bonds ≥ 0.5 Å	0
RMSD[b] on backbone atoms (pairwise, Å)	
Global	0.27
Ramachandran analysis	
Most favoured region	77.3%
Allowed region	22.7%
Generously allowed	0%
Disallowed	0%
Energies (kcal.mol^{-1})[c]	
Electrostatics	-1211 ± 10
Van der Waals	-280 ± 4
Total energy	-1243 ± 16
Residual NOE energy	10 ± 2

[a] Introduced as covalent bonds after convergence of the first runs of calculations.

[b] Calculated with CCpNMR.

[c] Calculated with the standard parameters of ARIA and given as mean ± standard deviation.

Figure 3 represents the overall fold of AmmTx3. As attested by the pairwise RMSD on the backbone atoms, the structure is very well defined and composed of an α-helix (14-20) and a 3-stranded β-sheet (2-4, 26-29, 32-35) (Table 1), organized into the well-known CSαβ motif [21] that is typical of this family of scorpion toxins.[22]

1.3. Biological activity of AmmTx3

We next assessed whether AmmTx3-NCL was functional and showed identical activity to AmmTx3 that was prepared by classical SPPS. This would be expected as both peptides had similar HMQC spectra. K_v4.2 channels were co-expressed with DDP6S and KCHIP1 subunits in Cos-7 cells, as they were shown to contribute to AmmTx3 pharmacology,[7] and recorded using the automated synchropatch 384PE patch clamp system (Figure 4).

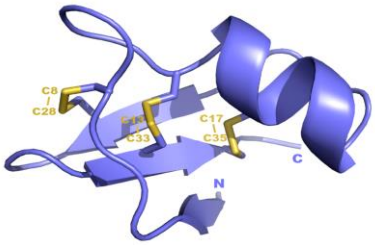

Figure 3. Schematic representation of AmmTx3 backbone, drawn with the PyMOL software (The PyMOL Molecular Graphics System, Version 2.0 Schrödinger, LLC). Disulfide bridges are represented in yellow, and cysteine residues are numbered to clearly identify the three disulfide bridges.

As shown, classical SPPS-prepared AmmTx3 and NCL-prepared AmmTx3 display very similar average $K_v4.2$ inhibition time courses, indicating that both peptides block with similar kinetics (Figure 4 A). Within 10 min $K_v4.2$ currents are almost completely blocked by the application of either 333 nM AmmTx3 or 333 nM AmmTx3-NCL (Figure 4 A, B). No statistical differences were found for the degree of maximum inhibition at 333 nM (90 ± 4% and 85 ± 5% for AmmTx3 produced by SPPS and NCL, respectively. P = 0.5421 Mann Whitney test). The effect of a lower peptide concentration on $K_v4.2$ activation properties was also investigated (Figure 4 C, D). None of the two toxins induced a shift in voltage-dependence of activation on partially blocked $K_v4.2$ currents at 33 nM AmmTx3 compared to control recordings in the absence of toxins (Figure 4 C). We concluded that both peptides were functional and identical in properties.

Finally, to demonstrate that our NCL-prepared AmmTx3 was also functional on native potassium channels, we tested the block of A-type K+ channels in a native living neuron in a brain slice using functional combined V_m and Ca^{2+} imaging as described in the experimental section. In the Purkinje neuron (PN) reported in Figure 5, the dendritic V_m and Ca^{2+} signals associated with a climbing fibre (CF) synaptic potential were recorded in control conditions and after local application of 1 µM AmmTx3-NCL. It has been shown that inactivation of A-type K+ channels enhances dendritic excitability and Ca^{2+} signals associated with CF synaptic potentials.[23] In agreement with this observation, application of AmmTx3-NCL substantially increased the dendritic V_m and Ca^{2+} signals associated with this stimulation protocol.

As expected, the biological activity of folded AmmTx3 prepared by NCL is coherent with expectations of channel block in native tissues.

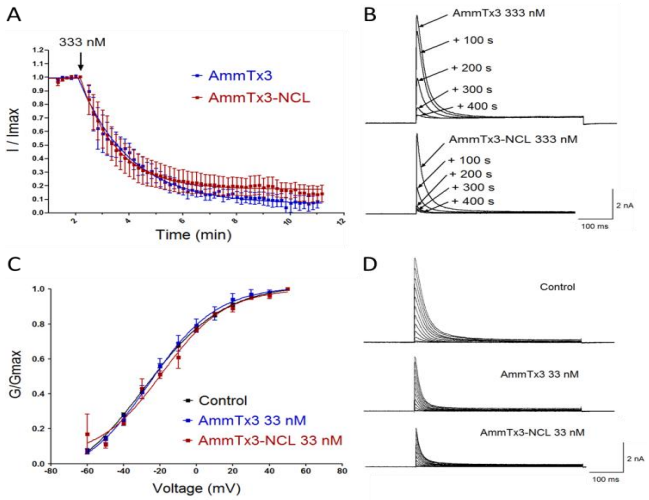

Figure 4. AmmTx3-NCL and AmmTx3 (produced by SPPS) equally block $K_v4.2$ channels. A) Average time course of $K_v4.2$ channel outward current block recorded at 70 mV following addition of either 333 nM AmmTx3 (blue trace, n = 6) or AmmTx3-NCL (red trace, n = 9). Error bars are SEM. B) Current traces from representative cells for $K_v4.2$ channel block recorded at different time points (100 s, 200 s, 300 s and 400 s) following addition of AmmTx3 (top) or AmmTx3-NCL (bottom). C) Kv4.2 activation curve (conductance-voltage relation G/Gmax) fitted with Boltzmann functions for control currents (black trace, n = 81), and following addition of 33 nM AmmTx3 (blue trace, n = 7) or AmmTx3-NCL (red trace, n = 2). Error bars are SEM. D) Representative traces in response to voltage clamp activation protocol recorded for control currents (top) and in the presence of 33 nM AmmTx3 (middle) or AmmTx3-NCL (bottom).

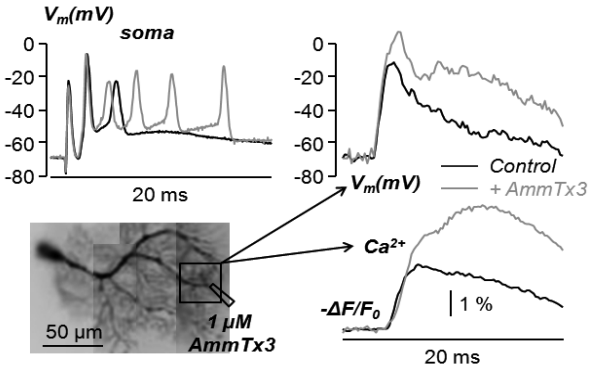

Figure 5. Specific effect of AmmTx3-NCL on the V_m and Ca^{2+} signals associated with the CF synaptic potential. Top-Left. CF synaptic potentials recorded with a patch electrode from the soma. Bottom-Left. Image of the PN with a dendritic recording region of interest outlined; the position of the pipette delivering 1 µM AmmTx3 is also indicated. Top-Right. Dendritic V_m associated with the CF input. Bottom-Right. -ΔF/F0 Ca^{2+} signals associated with the CF input. Black traces are in control conditions. Grey traces are after local application of AmmTx3-NCL.

2. Conclusions

In summary, AmmTx3 toxin was chemically produced via the NCL technique using peptide hydrazide as crypto-thioester. This approach provides an easy access to multi-milligram quantities of protein. We then determined the structure of AmmTx3 by using the NMR spectroscopy. The structural signature of this toxin is defined by the presence CSαβ motif that is typical of a family of scorpion toxins.[22] In parallel, complementary studies have shown biological activities of chemically-prepared AmmTx3 to be fully identical to the SPPS-mediated AmmTx3 synthetic peptide.

This methodology may be useful in order to carry out further biological studies as toxins represent potential therapeutic reagents but also for the production of interesting analogues.

3. Experimental Section

3.1. Synthesis of AmmTx3 via NCL.

20 mg of AmmTx3(1-12)-$NHNH_2$ (1 equiv., 12.3 µmol) was dissolved in 2.4 mL of 6 M Gn-HCl, 200 mM NaH_2PO_4 buffer at pH 3.0 and cooled in an ice/salt bath at -15 °C for 5 min. 245 µL of 0.5 M aqueous $NaNO_2$ solution (10 equiv.) were added and the mixture was agitated for 15 min at -15 °C. 29.6 mg of AmmTx3(13-37) (0.77 equiv.) and 206 mg of MPAA (100 equiv.) were dissolved in 2.4 mL of 6 M Gn-HCl, 200 mM Na_2HPO_4 buffer at pH 6.5 and added to the reaction mixture. The pH was adjusted to 6.8 and the reaction was mixed overnight under inert atmosphere at room temperature. 350 mg of tris(2-carboxyethyl)phosphine (TCEP) (100 equiv.) were dissolved in 15 mL of 6 M Gn-HCl solution, the pH was adjusted to 5.0, this solution was added to the reaction mixture and mixed during 30 min. The pH was lowered with 500 µL of TFA and the mixture was washed 4 times with 20 mL of Et_2O and purified by preparative RP-HPLC. After lyophilization, 20.1 mg of pure linear AmmTx3 were obtained. Yield 46%. MS calculated 3825.91; found 3825.83.

3.2. Folding of AmmTx3.

6.8 mg of linear AmmTx3 obtained by NCL was dissolved in 2 mL of a solution containing 0.1 % formic acid in H_2O and added dropwise to 35 mL of 0.2 M Tris.HCl buffer at pH 8.2 while stirring. The mixture was mixed gently for 48 h at room temperature, acidified with formic acid and purified by semi-preparative RP-HPLC. After lyophilization 3.2 mg of pure folded AmmTx3 were obtained. Yield 48 %. Purity 96 %. MS calculated 3819.87; found 3819.77.

3.3. NMR Experiments.

Samples of 1.2 $mmol.l^{-1}$ of AmmTx3 produced by NCL (1.0 mg dissolved in 220 µL of H_2O/D_2O (90/10) solution, pH = 4.5) and 0.6 mmol.l-1 of AmmTx3 produced by SPPS (0.5 mg dissolved in 220 µL of H_2O/D_2O (90/10) solution, pH = 4.5) were used for NMR experiments. All NMR spectra were recorded in 3 mm tubes on a BRUKER 700 Mhz NMR spectrometer equipped with a TCI cryoprobe, at 298 K: homonuclear 2D-COSY, -TOCSY (80 ms) and -NOESY (160 ms), and heteronuclear 1H-15N SoFast-HMQC with natural abundancy (4096 scans). All spectra were processed with Bruker's TopSpin3.2 software and analysed with CcpNMR software.[24]

3.4. Structure Calculations of AmmTx3-NCL.

Sequential assignments of AmmTx3 produced *via* NCL were carried out following classical procedure; distance constraints were deduced from the volume integration of NOE correlations and introduced into the standard iterative calculation process of the Aria2.3 software.[25] For each Aria run, 500 structures per iteration were calculated, and 250 structures were performed in the final iteration in water. For the two first runs, ambiguous intersulfur constraints were introduced, an option assuming that a given half-cystine is part of a bridge without supposing a particular partner, then allowing all combinations of pairing. In the further Aria runs, after convergence of the calculation, covalent bonds between sulphur atoms involved in each defined bridge were introduced. Moreover, constraints corresponding to the H-bonds observed within the β-sheet were added. Finally, ten of the final structures in agreement with all the experimental data and with standard covalent geometry were selected. The quality of the structures was evaluated using the PROCHECK3.5 software.[26]

3.5. Constructs and transfections.

The mouse pCMV-Script-Kv4.2 cDNA (NM_019697) was a generous gift from Dr. Jeanne M. Nerbonne (Washington University School of Medicine, St. Louis) and was previously described.[27] The human pCMV6-Entry-KCNIP1 (NM_014592) construct was purchased from Origene (Origene Technologies, Rockville, USA). The human pRC/RSV-DPP6S construct was a generous gift from Dr. Keiji Wada. The pEGFP-N1 plasmid was from Clontech Laboratories.

10xCOS-7 cells were transiently transfected using the OC-100 processing assemblies from the Maxcyte STX electroporation system (MaxCyte, Gaithersburg, MD) and used following the manufacturer's instructions. Co-transfections were performed as follows: 2 µg $K_v4.2$ plasmid, 6 µg DPP6S plasmid, 1 µg KCHIP1 plasmid and 1 µg eGFP plasmid. Transfected cells were plated onto P100 dishes and grown in DMEM supplemented with 10% FBS, 1% L-glutamine, 1% penicillin/streptomycin, at 37°C with 5% CO_2. Cells were used for recordings 48 h after transfection.

3.6. Automated patch-clamp recording.

Automated patch-clamp recordings were performed using the SynchroPatch 384PE (Nanion Technologies GmbH, Munich, Germany). Single-hole high-resistance chips (~10 MΩ) were used for the experiments. Before experiments, cells were washed with PBS and detached with trypsin-EDTA for 3 min. Trypsin was blocked with complete medium containing 10% FBS serum. Cells were then centrifuged 5 min at 900 rpm, and resuspended in patch-clamp extra-fill solution (composition in mM: NaCl 140, KCl 4, glucose 5, HEPES 10 (pH 7.4, NaOH)) for a 2 x 10^5 cells/mL final density. The cell suspension was maintained at 10°C and shaked in a hotel reservoir prior to patch-clamp experiment. Whole-cell recordings were carried out at room temperature. Pulse generation and data collection were performed with PatchController384 V1.5.2 and DataController384 V1.5.0. Recordings were performed using an extracellular solution

containing (in mM) : NaCl 80, NMDG 60, KCl 40, $CaCl_2$ 2, $MgCl_2$ 1, glucose 5, HEPES 10 (pH 7.4, NaOH). Intracellular solution contained (in mM) : KF 60, K-gluconate 50, KCl 30, NaCl 10, HEPES 10, HEDTA 10 (pH 7.2, KOH). For pharmacological experiments, compounds were first resuspended in milliQ water at a 1 mM stock concentration and then diluted in extracellular solution to different experimental concentrations.

For pharmacological investigation, currents were triggered with single step protocols. Holding potential was set at -90 mV and a 70 mV step was applied during 500 ms. Currents were recorded until they became stable. Sweep to sweep interval was 10 s. For voltage-dependent activation, holding potential was set at -90 mV and a series of test pulses from -60 mV to +50 mV was applied in 10 mV increments with a 7 s sweep to sweep interval.

3.7. Data analyses and statistics.

Electrophysiological data were analysed using the synchropatch 384PE datacontrol software version 1.5.0 and represented and statistically analysed using GraphPad Prism 5.02.

3.8. Evaluation of AmmTx3 effects on living neurons.

The Cerebellar slice from a 25 postnatal days old C57Bl6 mouse was prepared as described in a recent report [28] with procedures approved by the Isere prefecture (Authorisation n. 38 12 01). The solutions and the equipment utilized were those described in other previous reports.[29] The patch clamp recording from a Purkinje neuron (PN) was performed to load the cell with the voltage-sensitive dye was JPW1114 and with 1 mM of the low-affinity Ca^{2+} indicator FuraFF, to combine dendritic membrane potential (V_m) and Ca^{2+} fluorescence recordings.[30] In particular, V_m fluorescence was calibrated in absolute values (in mV) using an established procedure,[31] and corrected for the junction potential (-11 mV) as previously estimated.[32] Ca^{2+} signals were expressed as negative fractional change of fluorescence ($-\Delta F/F0$). Climbing fibre (CF) synaptic potentials were elicited by brief current pulses, of 5-20 µA amplitude and 100 µs duration delivered by a pipette placed near the recording cell. AmmTx3 was locally applied by pressure using a pipette placed near a distal dendritic region.

Acknowledgements

This work was supported by the Agence Nationale de la Recherche (ANR) LabEx "Arcane" support (ANR-11-LABX-0003-01) and LabEx "Ion Channels, Science and Therapeutics" (ANR-11-LABX-0015). MDW acknowledges financial support from Fondation Leducq, Région Pays de la Loire and FEDER. CZ acknowledges the Association Nationale de la Recherche et de la Technologie (ANRT) for its PhD financial support.

Supplementary Material

Supplementary data associated with this article can be found, in the online version, at

References and notes

1. Koh, C. Y. ; Kini R. M. *Toxicon* **2012**, *56*, 497–506.
2. Willians, J. A.; Days, M.; Heavners, J. E. *Expert Opin. Pharmacother.* **2008**, *9*, 1575–1583.
3. Norton, R. S.; Pennington, M. W.; Wulff, H. *Curr. Med. Chem.* **2004**, *11*, 3041–3052.
4. (a) Ahrén, B. *Curr. Diab. Rep.* **2003**, *5*, 365–372. (b) Holz, G. G.; Chepurny, O. G. *Curr. Med. Chem.* **2003**, *10*, 2471–2483.
5. (a) Barrese, V.; Stott, J. B.; Greenwood, I. A. *Annu. Rev. Pharmacol. Toxicol.* **2018**, *58*, 625–648. (b) Zhao, W.; Chen, Y. *Curr. Top. Med. Chem.* **2016**, *16*, 1877–1885. (c) Mathie, A.; Veale, E. L. *Pflugers Atch.* **2015**, *467*, 931–943.
6. Aidi-knani, S.; Regaya, I.; Amalric, M.; Mourre, C. *Behav. Pharmacol.* **2015**, *26*, 91–100.
7. Maffie, J. K.; Dvoretskova, E.; Bougis, P. E.; Martin-Eauclaire, M.-F.; Rudy, B. *J. Physiol.* **2013**, *591*, 2419–2427.
8. Vacher, H.; Alami, M.; Crest, M.; Possani, L. D.; Bougis, P. E.; Martin-Eauclaire, M.-F. *Eur. J. Biochem.* **2002**, *269*, 6037–6041.
9. (a) Raibaut, L. ; Ollivier, N. ; Melnyk, O. *Chem. Soc. Rev.* **2012**, *41*, 7001–7015. (b) Dawson, P. E.; Kent, S. B. H. *Annu. Rev. Biochem.* **2000**, *69*, 923–960.
10. De Rosa, L. ; Russomanno, A. ; Romanelli, A. ; Domenico D'Andrea, L. *Molecules* **2013**, *18*, 440–465.
11. (a) Ollivier, N.; Dheur, J.; Mhidia, R.; Blanpain, A.; Melnyk, O. *Org. Lett.* **2010**, *12*, 5238−5241. (b) Pattabiraman, V. R.; Ogunkoya, A. O.; Bode, J. W. *Angew. Chem., Int. Ed.* **2012**, *51*, 5114−5118.(c) Wang, J.-X; Fang, G.-M.; He, Y.; Qu, D.-L.; Yu, M.; Hong, Z.-Y.; Liu, L. *Angew. Chem. Int. Ed.* **2015**, *54*, 2194−2198. (d) Terrier, V. P.; Adihou, H.; Arnould, M.; Delmas, A. F.; Aucagne., V. *Chem. Sci.* **2016**, *7*, 339−345.
12. Fang, G.-M.; Li, Y.-M.; Shen, F.; Huang, Y.-C.; Li, J.-B.; Lin, Y.; Cui, H.-K.; Liu, L. *Angew. Chem. Int. Ed.* **2011**, *50*, 7645–7649.
13. Huang, Y.-C.; Fang, G.-M.; Liu, L. *Natl. Sci. Rev.* **2016**, *3*, 107–116.
14. Mlayah-Bellalouna, S.; Dufour, M.; Mabrouk, K.; Mejdoub, H.; Carlier, E.; Othman, H.; Belghazi, M.; Tarbe, M.; Goaillard, J. M.; Gigmes, D.; Seagar, M.; El Ayeb, M.; Debanne, D.; Srairi-Abid, N. *Toxicon* **2014**, *92*, 14–23.
15. Hackeng, T. M.; Griffin, J. H.; Dawson, P. E. *Proc. Natl. Acad. Sci. USA* **1999**, *96*, 10068–10073.
16. Isidro-Llobet, A.; lvarez, M. A.; Albericio, F. *Chem. Rev.* **2009**, *109*, 2455–2504.
17. Zheng, J.-S.; Tang, S.; Qi, Y.-K.; Wang, Z-P.; Liu, L. *Nat. Protoc.* **2013**, *8*, 2483–2495.
18. HPLC conditions: peptide elution was performed at a flow rate of 3 mL/min with a 5-65 % gradient of solvent B over 10 min with a Chromolith® High Resolution column (RP-18e, 150 Å, 10 x 4.6 mm). Solvents A and B were respectively 0.1% TFA in H_2O and 0.1% TFA in MeCN.
19. HPLC conditions: peptide elution was performed at a flow rate of 1 mL/min with a 5-65% gradient of solvent B over 12 min with a Agilent AdvanceBio Peptide column (120 Å, 2.7 µm, 100 x 2.1 mm).

20. Schanda, P.; Brutscher, B. *J. Am. Chem. Soc.* **2005**, *127*, 8014–8015.
21. Cornet, B.; Bonmatin, J. M.; Hetru, C.; Hoffmann, J. A.; Ptak, M.; Vovelle, F. *Structure* **1995**, *3*, 435–448.
22. de la Vega, C. R. R.; Possani, L. D. *Toxicon* **2004**, *43*, 865–875.
23. Otsu, Y.; Marcaggi, P.; Feltz, A.; Isope, P.; Kollo, M.; Nusser, Z.; Mathieu, B.; Kano, M.; Tsujita, M.; Sakimura, K.; Dieudonne, S. *J. Neurosci.* **2014**, *84*, 137–151.
24. Vranken, W. F.; Boucher, W.; Stevens, T. J.; Fogh, R. H.; Pajon, A.; Llinas, M.; Ulrich, E. L.; Markley, J. L.; Ionides, J.; Laue, E. D. *Proteins* **2005**, *59*, 687–696.
25. Rieping, W.; Habeck, M.; Bardiaux, B.; Bernard, A.; Malliavin, T. E.; Nilges, M. *Bioinformatics* **2007**, *23*, 381–382.
26. Laskowski, R. A.; MacArthur, M. W.; Moss, D. S.; Thornton, J. M. *J. App. Cryst.* **1993**, *26*, 283–291.
27. Marionneau, C.; Carrasquillo, Y.; Norris, A. J.; Townsend, R. R.; Isom, L. L.; Link, A. J.; Nerbonne, J. M. *J. Neurosci.* **2012**, *32*, 5716–5727.
28. Ait Ouares, K.; Jaafari, N.; Canepari, M. *J. Neurosci. Methods* **2016**, *268*, 66–77.
29. Jaafari, N.; Canepari, M. *J. Physiol.* **2016**, *549*, 967–983.
30. Vogt, K. E.; Gerharz, S.; Graham, J.; Canepari, M. *J. Physiol.* **2011**, *589*, 489–494.
31. Canepari, M.; Vogt, K. E. *PLoS ONE* **2008**, *3*, e4011.
32. Canepari, M.; Willadt, S.; Zecevic, D.; Vogt, K. E. *Biophys. J.* **2010**, *98*, 2032–2040.